



HAL
open science

Tunable acetylene sorption by flexible catenated metal–organic frameworks

Mickaele Bonneau, Christophe Lavenn, Jia-Jia Zheng, Alexandre Legrand, Tomofumi Ogawa, Kunihisa Sugimoto, François-Xavier Coudert, Regis Reau, Shigeyoshi Sakaki, Ken-Ichi Otake, et al.

► **To cite this version:**

Mickaele Bonneau, Christophe Lavenn, Jia-Jia Zheng, Alexandre Legrand, Tomofumi Ogawa, et al.. Tunable acetylene sorption by flexible catenated metal–organic frameworks. *Nature Chemistry*, 2022, 14 (7), pp.816-822. 10.1038/s41557-022-00928-x . hal-03648780

HAL Id: hal-03648780

<https://hal.science/hal-03648780>

Submitted on 21 Apr 2022

HAL is a multi-disciplinary open access archive for the deposit and dissemination of scientific research documents, whether they are published or not. The documents may come from teaching and research institutions in France or abroad, or from public or private research centers.

L'archive ouverte pluridisciplinaire **HAL**, est destinée au dépôt et à la diffusion de documents scientifiques de niveau recherche, publiés ou non, émanant des établissements d'enseignement et de recherche français ou étrangers, des laboratoires publics ou privés.

Tunable acetylene sorption by flexible catenated metal–organic frameworks

Mickaele Bonneau¹, Christophe Lavenn², Jia-Jia Zheng^{1,3}, Alexandre Legrand¹, Tomofumi Ogawa², Kunihisa Sugimoto^{1,4}, Francois-Xavier Coudert⁵, Regis Reau⁶, Shigeyoshi Sakaki³, Ken-ichi Otake¹ & Susumu Kitagawa^{1*}

¹ Institute for Integrated Cell-Material Sciences (WPI-iCeMS), Kyoto University, Sakyo-ku, Kyoto 606- 8501, Japan

² Air Liquide Laboratories, Innovation campus Tokyo, 2-2 Hikarinooka, Yokosuka, Kanagawa, 239-0847 Japan

³ Element Strategy Initiative for Catalyst and Batteries, Kyoto University, Goryo-Ohara 1-30, Nishikyo-ku, Kyoto 615-8245, Japan

⁴ Japan Synchrotron Radiation Research Institute/ SPring-8, Kouto, Sayo, Hyogo 679-5198, Japan

⁵ Chimie Paris Tech, PSL University, CNRS, Institut de Recherche de Chimie Paris, 75005 Paris, France

⁶ Air Liquide R&D, Innovation Campus Paris 1, Chemin de la Porte des Loges 78350 Les Loges-en-Josas, France.

ABSTRACT. The safe storage of flammable gases, such as acetylene, is essential for current industrial purposes. However, the narrow pressure and temperature range required for the industrial use of pure acetylene ($100 < P < 200$ kPa at 298 K) and its explosive behaviour at higher pressures make its storage and release challenging. Flexible metal–organic frameworks (MOFs) that exhibit a gated adsorption/desorption behaviour — in which guest uptake/release occur above threshold pressures, usually accompanied by framework deformations — have

shown promise as storage adsorbents. Herein, the pressures for gas uptake and release of a series of zinc-based mixed-ligand catenated MOFs were controlled by functionalizing the two ligands as well as changing their ratio. This affects the deformation energy of the framework, which in turn controls the gated behaviour. The materials offer good performances for acetylene storage with a usable capacity of ~ 90 v/v (77 % of the overall amount) at 298 K and under a practical pressure range (100–150 kPa).

The development of new technologies for efficient gas storage at ambient pressure can improve safety and provide new possibilities for gas cylinder design. The usable gas capacity, which differs from the maximum quantity adsorbed, under mild pressure and temperature conditions is another concern for researchers. In contrast to gases such as carbon dioxide, methane, oxygen, and nitrogen, which have wider compression pressure tolerances, pure acetylene gas is challenging to handle and safely store due to its explosive behaviour when compressed over 200 kPa at room temperature. Consequently, in the last century, cylinders have been filled with acetylene dissolved at high pressure ($P > 1500$ kPa) in a solvent such as acetone.¹⁻³ However, such acetylene commercial set-up could contaminate the acetylene gas. When cylinders are filled with pure acetylene gas at 200 kPa (safe pressure), it only allows the release of 50 % of its total capacity at 100 kPa (limit pressure for the gas to flow spontaneously), keeping 50 % unused, which is not economically useful and potentially dangerous. The creation of porous materials capable of delivering large quantities of pure acetylene in a highly narrow pressure range (100–150 kPa) at room temperature is therefore essential.⁴

As a potential solution, porous materials, particularly metal-organic frameworks (MOFs) or porous coordination polymers (PCPs), possess inherent voids that allow the storage and delivery

of large amounts of gases.⁵⁻⁸ In contrast to rigid materials showing a Langmuir type I isotherm, flexible MOFs, also called soft porous crystals (SPCs), possess both ordered network and structural transformability, resulting in a sigmoidal S-shape isotherm and higher usable storage capacity (USC) when the gate pressures are in the desired working pressure range (**Fig. 1**).⁹⁻¹²

The flexibility depends not only on the binding capacity and mobility of unit ligands and metal ions but also on other factors, including the deformation of the entire framework as a result of the guest molecules in the pores.¹³⁻¹⁵ Strategies using ligand functionalisation have been developed to investigate the behaviour and properties of flexible MOFs.¹⁶⁻²¹ Still, none of them focused on gas storage and especially sensitive gas, which mandates strict temperature and pressure conditions.²²⁻²⁷

Regarding acetylene storage, rigid and flexible MOFs have demonstrated high adsorption capacities at 298 K and 100 kPa. However, the desorption pressure does not match the acetylene storage requirements for safe handling described above. All the MOFs reported for their high acetylene capacities were recorded at a pressure of 100 kPa, which is below the ideal working pressure range.²⁸⁻³² Speculative values were also calculated for acetylene adsorption at high pressure ($P > 3500$ kPa), far above the explosion limit for acetylene.³² Herein, we demonstrate the optimum pressure range for stable acetylene storage while maintaining high deliverable capacity.³³⁻³⁶ To the best of our knowledge, acetylene sorption isotherms on MOFs at a pressure range between 100–150 kPa have not been reported so far.

We used a doubly catenated structure, i.e., interpenetrated or two-fold interlocked, as an SPC candidate; $[\text{Zn}_2(\text{bdc})_2(4,4'\text{-bpy})]$ (bdc = 1,4-benzenedicarboxylic acid; 4,4'-bpy = 4,4'-bipyridine) (**Zn-CAT**), where the mutual dislocation of the two identical framework motifs can introduce acetylene, displaying a sigmoidal sorption isotherm. The gate-opening and -closing

pressures (P_{go} and P_{gc}) depend on the deformation energy to create space, attributed to the interaction between the two interpenetrating frameworks.^{37,38} Therefore, the isotherm can be controlled by the steric and electronic properties of the organic linker (L) of the framework. At a certain temperature, T , the isotherm is a function of P and L as $A_T = F(P, L)$ (**Fig. 1**). The introduction of different ratios of functionalised **bdc-X** linkers ($X = -NO_2$ or $-NH_2$) allows the optimization of the sigmoidal sorption at temperature storage and 100 kPa release of acetylene. The strategy of deformation energy control, as devised for acetylene, is also applicable to CO_2 , O_2 , and CH_4 gases in which lower filling and release pressures are preferable for the safer use of the gas cylinder.

Results and Discussion

Synthesis and characterisation

A series of **Zn-CAT** derivatives composed of a mixture of **bdc** and a substituted **bdc-X** ($X = -NO_2$ or $-NH_2$) ligands were synthesised with precise control of the **bdc/bdc-X** ratio (**Figs. 2a–c** and Supplementary **Fig. 1**).³⁷ The final linker ratio of these $[Zn_2(bdc)_{2-a}(bdc-X)_a(bpy)]$ materials (with **a** varying from 0 to 2) was confirmed by 1H NMR and showed almost no deviation from the linker ratio expected from the introduced mixture (**Fig. 2c** and Supplementary **Figs. 2–14**). The samples were designated according to **Zn-CAT-(X)_n**, that is, the functional moiety ($X = -NH_2, -NO_2$) and molar percent ($n = 0–100\%$) for clarity. All materials were thermally stable up to 623 K, as observed by thermogravimetric analysis (TGA) (Supplementary **Figs. 15–17**). The SEM images of the as-synthesised samples were then analysed and exhibited homogeneity of particle sizes in the micrometre range (Supplementary **Figs. 18–19**). Powder X-ray patterns (PXRD), infrared analysis (IR), UV-vis and crystal structures of the as-synthesised and activated samples confirmed the purity of all materials as well as their isostructural nature

(Supplementary **Figs. 20–26** and **Tables 1–2**). Interpenetrated **Zn-CAT** shows a dynamic transition from the closed (when the structure is completely evacuated from guests) to the open form (when a specific gas pressure or temperature is applied).³⁹ Thus, the gas sorption properties of the **Zn-CAT-(X)_n** series were investigated.

First, **Zn-CAT-(X)_n** samples were confirmed to behave as a solid solution; that is, the ligands were homogeneously distributed within the backbone structures (Supplementary **Fig. 27**).^{40,41} The influence of the ratio of linker mixture on the P_{go}/P_{gc} pressures was determined from single gas-adsorption measurements performed at different temperatures and pressures (**Fig. 3** and Supplementary **Figs. 28–36**). Acetylene physisorption of pristine **Zn-CAT** at 273 K showed $P_{go} = 44$ kPa and $P_{gc} = 19$ kPa with an excess amount of 2.87 mol.mol⁻¹ of acetylene adsorbed (**Fig. 3**).³⁹ When **Zn-CAT-(NH₂)_n** is used, a shift in P_{go} from 48 to 83 kPa was observed as n increased from 5 to 60% (**Fig. 3a**). In contrast, for **Zn-CAT-(NO₂)_n**, the gate-opening pressure shifted to a lower pressure when n increased from 5 to 100 % (from $P_{go} = 31$ kPa to $P_{go} = 1$ kPa) (**Fig. 3b**). The plot of the gate-opening and -closing pressures as a function of the molar percentage of amino groups in **Zn-CAT-(NH₂)_n** suggests that P_{go} increases exponentially with the amount of **bdc-NH₂** incorporated (**Fig. 3c**). At a higher molar percentage ($n > 60\%$) of **bdc-NH₂**, P_{go} was not observed below 100 kPa; however, the value can be extrapolated from the exponential fit of the lower molar percentage data points and later confirmed by high-pressure measurements (**Fig. 3** and Supplementary **Figs. 37–44**). This extrapolation is possible due to the exponential trend observed at a lower temperature (195 K), where all P_{go} values can be determined for high amino loading (Supplementary **Figs. 28–29**). Additionally, the nitro group exhibited a significant impact on the exponential decay of P_{go} as a function of n (**Fig. 3d**).

***In-situ* gas sorption studies**

The structure of **Zn-CAT**, **Zn-CAT-(NH₂)₁₀₀**, and **Zn-CAT-(NO₂)₁₀₀** were also characterized by *in situ* PXRD under various acetylene pressures at 195 K (Supplementary **Fig. 45**) to further investigate the effect of **bdc** substitution and phase transformations.

Increasing the gas pressure resulted in a transition from a close to open phase structure, which occurred at different pressures for the three samples. The gate-opening pressures, which correspond to the phase transition observed on the PXRD patterns, were observed at $P_{go} = 0.04$, 0.21, and 1.16 kPa for **Zn-CAT-(NO₂)₁₀₀**, **Zn-CAT**, and **Zn-CAT-(NH₂)₁₀₀**, respectively. The difference in the parent structure can explain this difference. Below P_{go} , the PXRD patterns of activated MOFs (closed form) for **Zn-CAT-(NH₂)₁₀₀** and **Zn-CAT-(NO₂)₁₀₀** show a decrease and increase in the volume of the cell, respectively, compared to pristine **Zn-CAT**, as seen from the shift of the 100 peak. These results were confirmed by the crystal structure obtained from X-ray diffraction experiments (Supplementary **Table 1–2**).³⁸ The cell volume of activated **Zn-CAT-(NO₂)₁₀₀** (715.9 Å³) is higher than that of **Zn-CAT** (703.6 Å³) and **Zn-CAT-(NH₂)₁₀₀** (701.9 Å³), which can be attributed to i) the softer interaction of **-NO₂** groups with the metal nodes and ii) the steric hindrance of the **-NO₂** moiety, which further separates the aromatic part of the ligand. Therefore, the stabilisation of the structure through π - π interactions is reduced, as observed for pristine MOF.⁴²

For **Zn-CAT-(NH₂)₁₀₀**, the higher pressure needed for the gate opening to occur is explained by the initially more contracted structure owing to interactions between **-NH₂** moieties and oxygen atoms from the metal paddlewheel.³⁸ Finally, all MOF structures are entirely open in the higher pressure range, and they display similar diffraction patterns (Supplementary **Figs.**

45d–f). Considering that the open and closed forms of each material are isostructural, the difference in the gate-opening pressure is attributed to the functionalised **bdc-X** linker.

Theoretical investigations of the gate-opening behaviour

To rationalise the effect of linker on the thermodynamics of the gate-opening process, we applied theoretical thermodynamic models to the adsorption isotherms of **Zn-CAT** and its derivatives (Supplementary information).^{43,44} Researchers have previously shown that a simple two-phase model provides a good description of gate opening in interpenetrated frameworks. The gate opening is an adsorption-driven first-order phase transition from a nonporous phase to a microporous phase. Here, the “open phase” adsorption is described by a Langmuir-type fit of isotherms for all materials at 273 K. The free energy difference (ΔF) associated with the gate-opening process have been calculated based on the adsorption and desorption isotherms (see Supplementary Information for the equations). This value indicates that **Zn-CAT** exhibits a relatively small free energy difference ($\Delta F = 5.2$ kJ/mol) between the two phases (here, all energies are reported per unit cell). This value is slightly larger, but of a similar order of magnitude, than those of other gate-opening materials, such as $[\text{Cu}(4,4'\text{-bpy})(\text{dhbc})_2]\text{H}_2\text{O}$, which has a ΔF of approximately 4 kJ/mol).^{21,45} The relatively small free energy difference between the two phases explains why the material readily opens upon adsorption of small guests.

However, the introduction of $-\text{NO}_2$ and $-\text{NH}_2$ substituents leads to a decrease in ΔF (see Supplementary **Table 3**). The impact of $-\text{NH}_2$ was determined to be smaller than that of $-\text{NO}_2$. The more pronounced decrease in ΔF of **Zn-CAT-(NO₂)₁₀₀** is attributed to the repulsive interaction of the $-\text{NO}_2$ groups in the closed phase. Owing to the smaller energetic cost for gate opening, the opening is easier and occurs at lower gas pressures. This is particularly noticeable in the **Zn-CAT-(NO₂)₁₀₀** phase, where the free energy difference is almost zero, which implies that

the material is truly bistable. Minute amounts of adsorbate trigger the gate-opening transition. This effect was more complex when $-\text{NH}_2$ groups are present. The introduction of $-\text{NH}_2$ groups in **Zn-CAT** decreased ΔF but did not lead to a decrease in the gate-opening (and closing) pressure. The effect is smaller than that of the $-\text{NO}_2$ groups because $-\text{NH}_2$ is a less bulky substituent. Therefore, the change in ΔF is not the dominant factor, and the driving force is the evolution of affinity in the open phase, discussed in detail later in the paper.

These results suggest the possibility of purposefully controlling the gate-opening and closing pressure by introducing different ratios of functional groups. Additionally, the dependence of gate-opening and closing on the molar ratio of amino or nitro functional groups is not unique to acetylene. Still, it is also applicable to CO_2 , O_2 , and CH_4 , demonstrating the method's versatility (Supplementary **Figs. 30–36**).

Notably, the total adsorbed capacity does not considerably change for all **Zn-CAT-(NH₂)_n** compared to that of pristine **Zn-CAT** for acetylene gas at 273 K (**Fig. 3c**). The total adsorption capacity at higher loading in the **Zn-CAT-(NH₂)_n** series was recorded at a lower temperature ($T = 195$ K), demonstrating that the total capacity did not decrease for all **Zn-CAT-(NH₂)_n** series (Supplementary **Fig. 28–29**). Conversely, the capacity decreases up to 15% for **Zn-CAT-(NO₂)₁₀₀** (from $2.73 \text{ mol}\cdot\text{mol}^{-1}$ to $2.32 \text{ mol}\cdot\text{mol}^{-1}$). This difference is expected due to the bulkier nitro moiety (VDW surface area **bdc-NO₂** = 249.2 \AA^2) compared to the amino moiety (VDW surface area **bdc-NH₂** = 223.3 \AA^2).

To elucidate the origin of the counter-intuitive observation that the gate-opening pressure decreases after introducing a $-\text{NO}_2$ group into **Zn-CAT** but increases after introducing an $-\text{NH}_2$ group, quantum chemical calculations were carried out (see Supplementary Information for computational details). For clarity, only C_2H_2 adsorption onto pristine **Zn-CAT** and fully

substituted MOFs, that is, **Zn-CAT-(NH₂)₁₀₀** and **Zn-CAT-(NO₂)₁₀₀**, were considered. As shown in **Table 4** of the Supplementary Information, the binding energy (*BE*) of C₂H₂ with MOFs increased from **Zn-CAT-(NH₂)₁₀₀** (−9.3 kcal/mol) > **Zn-CAT** (−9.9 kcal/mol) > **Zn-CAT-(NO₂)₁₀₀** (−10.6 kcal/mol), where a more negative *BE* value indicates stronger C₂H₂ adsorption with increased energy stabilisation. The results suggest that C₂H₂ adsorption begins to occur at a higher pressure for **Zn-CAT-(NH₂)₁₀₀** but at lower pressure for **Zn-CAT-(NO₂)₁₀₀**, consistent with the experimental results.

The *BE* was decomposed into the interaction energy (*E_{int}*) between the MOF and C₂H₂ molecules and that of the adsorbed C₂H₂ molecules and the deformation energy (*E_{def}*) of the MOF structure by C₂H₂ adsorption. The *E_{int}* values were similar for C₂H₂ adsorption onto **Zn-CAT**, **Zn-CAT-(NH₂)₁₀₀**, and **Zn-CAT-(NO₂)₁₀₀**, which is reasonable because the adsorption positions of C₂H₂ in these MOFs are similar (Supplementary **Fig. 46**). However, *E_{def}* differs considerably and is of the same order as that of *P_{go}*. The larger *E_{def}* for **Zn-CAT-(NH₂)₁₀₀** indicates that the introduction of the −NH₂ group into **Zn-CAT** results in a less flexible framework; thus, the gate-opening pressure increases. The less flexible framework occurs due to the hydrogen-bonding interactions of the −NH₂ group with the neighbouring **bpy** and carboxylate ligands (Supplementary **Fig. 47a**). The hydrogen-bonding interaction between the −NH₂ group and the **bpy** ligand weakened after C₂H₂ adsorption, confirmed by the increase in the NH₂-**bpy** distance (Supplementary **Fig. 47a-b**). For **Zn-CAT-(NO₂)₁₀₀**, the introduced −NO₂ group results in a repulsive interaction with the carboxylate ligand (Supplementary **Fig. 47c**) in the guest-free structure. Consequently, the framework flexibility is increased to reduce the repulsive interaction, explaining the smaller *E_{def}* of **Zn-CAT-(NO₂)₁₀₀** than that of pristine **Zn-CAT**, hence decreasing the gate-opening pressure. Indeed, the −NO₂ groups do not exist in a

repulsive position after C₂H₂ adsorption (Supplementary **Fig. 47d**). These results indicate that introducing substituents into parent MOFs can tune the flexibility of MOFs and readily change the E_{def} of the framework upon gas adsorption, making it possible to control the gate-opening gas adsorption, as observed from the experimental results.

Optimal conditions

Owing to the insight into the structural dynamics of our system obtained from the combination of various characterisation techniques and theoretical calculations, the amino group efficiently adjusted both P_{go} and P_{gc} for practical use at different temperatures (**Fig. 4**). Due to the limitation of actual physisorption instruments to 100 kPa pressure, we built a system capable of recording the acetylene physisorption at a higher pressure than 100 kPa, which was not been seen before (Supplementary **Fig. 37**). The optimal compressed condition must not exceed 200 kPa due to the acetylene explosive behavior above this pressure. The discharge gas should happen above 100 kPa because the gas would not flow automatically below this pressure. Thus, it is possible, with this solid-solution system, to fill at low temperature to achieve high adsorption amount at low gate opening pressure while releasing at room temperature above 100 kPa. The optimal conditions for the safe handling and use of compressed pure acetylene gas were tested for **Zn-CAT-(NH₂)₆₀** with a maximum released gas of 66 v/v at 100 kPa and 310 K (which is 67 % of the cylinder content) and **Zn-CAT-(NH₂)₁₀₀**, which allowed the release of 77 % of the cylinder content (~ 90 v/v) at 100 kPa and 298 K (**Fig. 4** and Supplementary **Fig. 44**).

Our system has three main advantages compared to the state-of-the-art materials. First, when comparing the usable storage capacity of acetylene for **Zn-CAT-(NH₂)₁₀₀** with the reported MOFs, our material provides an USC of ~ 90 v/v at 150 kPa and degassing at 100 kPa, both at 298 K, which is the highest among the reported MOFs (**Fig. 4c** and Supplementary **Table**

5). Second, **Zn-CAT-(NH₂)₁₀₀** achieves 77% of the amount released at 100 kPa, which is a crucial indicator of safety, as the unused or trapped acetylene is potentially dangerous (**Fig. 4c**). Compared to the MOFs reported for their high adsorption capacity, all retained at least 50 % of acetylene in their pores. Third, the recyclability tests did not show any change in the uptake or release capacity, which is in contrast with the conventional zeolite-type adsorbents that cannot be reused without strong heating reactivation (Supplementary **Fig. 48-49**).

For industrial development, we demonstrated that our flexible MOF adsorbents exhibit the following practical advantages for storing acetylene compared to the current solvent compression method (**Fig. 4d**). High acetylene purity is achieved as no solvents that can degrade or contaminate are present. The functionalized **Zn-CAT-(X)_n** can compress large quantities of acetylene (~ 117 v/v) at less than 200 kPa, allowing the development of smaller gas containers at low pressure with filling controlled *via* a pressure gauge and not by mass. Compared to the solvent-free compression method, the adsorbed gas can be compressed in larger quantities in MOF pores (37-fold increase, **Fig. 4d**). Finally, the release pressure condition can be easily manageable with the % ratio of the amino group. Indeed, geographically different locations have different climates and thus different temperature regimes in which to operate the acetylene containers. Therefore, the tailor-designed of **Zn-CAT-(X)_n** solid solution offers tunable uptake/release pressures at a desired temperature for various gases.

Conclusion

Herein, we demonstrated the design of a functional MOF with practical gate pressures *via* a modification of the molecular framework. The designed system has a mechanism by which the substituent exchange of the ligand controls the gate pressures of the target guest molecule by

modulating the deformation energy of the interpenetrated framework. In the case of acetylene storage, these conditions were met using **Zn-CAT-(NH₂)₆₀** at 310 K and **Zn-CAT-(NH₂)₁₀₀** at 298 K, which allowed the release of more than 66 % of acetylene at 100 kPa. This method is versatile, as it uses readily available MOFs and achieves the required performance with only minor modifications. These results open the way for the application of flexible MOFs to the practical storage of targeted gases from the discovery of cooperative adsorption phenomena.

Acknowledgements

This work was supported by Air Liquide via the 2016 Air Liquide Scientific Challenge, a KAKENHI Grant-in-Aid for Specially Promoted Research (JP25000007), Scientific Research (S) (JP18H05262), and Early-Career Scientists (JP19K15584) from the Japan Society of the Promotion of Science (JSPS). Synchrotron XRD measurements were performed at the Japan Synchrotron Radiation Institute (JASRI), Super Photon ring-8 GeV (Spring-8) (Proposal numbers 2018B1820 and 2019A1136). We acknowledge iCeMS Analysis Centre for access to analytical facilities.

We are grateful to CNRS-Kyoto LIA "SMOLAB". In addition, we thank Air Liquide Japan, Dr. Patrick Ginet and Laurent Prost as well as the technical staff for advices and experimental assistance.

Author Contributions

S.K., C.L and R.R. formulated the project. M.B and C.L. synthesized the compounds and collected the gas adsorption data. M.B. and C.L analyzed all adsorption data. M.B and C.L. collected and analyzed the ¹H NMR, TGA, and powder X-ray diffraction data. K.O. and K.S. collected and analyzed the synchrotron X-ray diffraction data. A.L. and M.B. collected all SEM images UV-vis and IR data. F-X.C. performed the thermodynamics calculations. J.Z. and S.S.

performed the quantum chemical calculations. T.O. and C.L. build and collected the sorption data from the acetylene experimental set-up. M.B, K.O., A.L., J.Z., F-X.C, and S.K. wrote the paper, and all authors contributed to revising the paper.

Competing Interests statement

The authors declare no competing financial interests.

Figure Legends

Fig. 1 | Adsorption S-shape isotherms of flexible MOF depending on pressure and organic linker. A type I adsorption isotherm of rigid MOF is shown in gray for comparison. The functionalization of **Zn-CAT** with $-\text{NO}_2$ or $-\text{NH}_2$ groups leads to a shift in the gate pressure to the lower pressure (blue circles) or higher pressure range (red circles), respectively. The orange area represents the targeted practical range (100–150 kPa) for safe acetylene uses.

Fig. 2 | Presentation of the **Zn-CAT-(X)_n** derivatives as SPC candidate. a) Synthetic scheme of **Zn-CAT-(X)_n** materials. b) (Left) crystal structure of activated **MOF-508** along the b axis and (right) crystal structure of activated **Zn-CAT** along the c axis showing a pillar ligand connecting the 2D layers. c) Molar percentage of the **bdc-X** linker within the material obtained as a function of the molar percentage of **bdc-X** introduced in the reaction. The obtained ratio was estimated from the ^1H NMR spectra of digested sample available in the **Supplementary Fig. 2-14**.

Fig. 3 | Tunable acetylene uptake and release sorptions. a) Acetylene (C_2H_2) adsorption isotherms for all **Zn-CAT-(NH₂)_n** at 273 K. The **Zn-CAT** isotherm (black) was added for comparison. b) Acetylene (C_2H_2) adsorption isotherms for all **Zn-CAT-(NO₂)_n** at 273 K. The **Zn-CAT** isotherm (black) was added for comparison. c) Acetylene (C_2H_2) gate opening (green filled circle), predicted gate opening (light green filled circle) and closing (green empty circle) pressure for all **Zn-CAT-(NH₂)_n** at 273 K. Total capacity (orange filled square) as a function of mol% of $-\text{NH}_2$ in **Zn-CAT** if reached below 100 kPa. d) Acetylene (C_2H_2) gate opening (green filled circle) and closing (green, empty circle) pressure for all **Zn-CAT-(NO₂)_n** at 273 K. Total capacity (orange filled square) as a function of mol% of $-\text{NO}_2$ in **Zn-CAT** if reached below 100 kPa. The total capacities were collected from the maximum uptake obtained in the adsorption isotherm. The gate opening and closing pressures were calculated from the adsorption and desorption isotherm inflexions at 273K. The simulated gate opening pressure were extrapolated from the exponential growth function with rate constant parameter.

Fig. 4 | Efficiency of **Zn-CAT-(X)_n** for acetylene storage. Obtained (filled symbols) and predicted (empty symbols) gate **a)** opening and **b)** closing pressures of **Zn-CAT** and **Zn-CAT-**

$(\text{NH}_2)_n$ as a function of temperature. Gray square shows the best region for practical discharge pressure for acetylene gas release (100–150 kPa). c) Comparison of the usable storage capacities in function of discharge ratios for acetylene storage of reported MOFs. d) Comparison of commercialized acetylene cylinders with an estimated **Zn-CAT-(NH₂)₁₀₀** filler system.

References

- 1 Matsuda, R. *et al.* Highly controlled acetylene accommodation in a metal–organic microporous material. *Nature* **436**, 238-241, doi:10.1038/nature03852 (2005).
- 2 Safetygram 13, Acetylene. *Air Products and Chemicals Inc.* (2014).
- 3 Solvents for Acetylene Filling. *European Industrial Gases Association AISBL Doc. 225/19* (2019).
- 4 Martin Bulow, S. B., Dougill Norman, Douglas Parkyns, Wasyl Michael Sajik. Method and vessel for the storage of gas. United State patent (1999).
- 5 Kapelewski, M. T. *et al.* Record High Hydrogen Storage Capacity in the Metal–Organic Framework Ni₂(m-dobdc) at Near-Ambient Temperatures. *Chem. Mater.* **30**, 8179-8189, doi:10.1021/acs.chemmater.8b03276 (2018).
- 6 Li, B., Wen, H.-M., Zhou, W., Xu, Jeff Q. & Chen, B. Porous Metal-Organic Frameworks: Promising Materials for Methane Storage. *Chem* **1**, 557-580, doi:10.1016/j.chempr.2016.09.009 (2016).
- 7 Moghadam, P. Z. *et al.* Computer-aided discovery of a metal–organic framework with superior oxygen uptake. *Nat. Commun.* **9**, 1378, doi:10.1038/s41467-018-03892-8 (2018).
- 8 Vaidyanathan, R. *et al.* Direct observation and quantification of CO₂ binding within an amine-functionalized nanoporous solid. *Science (New York, N.Y.)* **330**, 650-653, doi:10.1126/science.1194237 (2010).
- 9 Horike, S., Shimomura, S. & Kitagawa, S. Soft porous crystals. *Nat. Chem.* **1**, 695-704, doi:10.1038/nchem.444 (2009).
- 10 Warren, J. E. *et al.* Shape Selectivity by Guest-Driven Restructuring of a Porous Material. *Angew. Chem. Int. Ed.* **53**, 4592-4596, doi:10.1002/anie.201307656 (2014).
- 11 Chang, Z., Yang, D.-H., Xu, J., Hu, T.-L. & Bu, X.-H. Flexible Metal–Organic Frameworks: Recent Advances and Potential Applications. *Adv. Mater.* **27**, 5432-5441, doi:10.1002/adma.201501523 (2015).
- 12 Schneemann, A. *et al.* Flexible metal–organic frameworks. *Chem. Soc. Rev.* **43**, 6062-6096, doi:10.1039/C4CS00101J (2014).
- 13 Zhang, J.-P. & Chen, X.-M. Optimized Acetylene/Carbon Dioxide Sorption in a Dynamic Porous Crystal. *J. Am. Chem. Soc.* **131**, 5516-5521, doi:10.1021/ja8089872 (2009).

- 14 Henke, S., Schneemann, A., Wütscher, A. & Fischer, R. A. Directing the Breathing Behavior of Pillared-Layered Metal–Organic Frameworks via a Systematic Library of Functionalized Linkers Bearing Flexible Substituents. *J. Am. Chem. Soc.* **134**, 9464-9474, doi:10.1021/ja302991b (2012).
- 15 Jiang, H.-L., Makal, T. A. & Zhou, H.-C. Interpenetration control in metal–organic frameworks for functional applications. *Coord. Chem. Rev.* **257**, 2232-2249, doi:doi.org/10.1016/j.ccr.2013.03.017 (2013).
- 16 Martí-Gastaldo, C. *et al.* Side-chain control of porosity closure in single- and multiple-peptide-based porous materials by cooperative folding. *Nat. Chem.* **6**, 343-351, doi:10.1038/nchem.1871 (2014).
- 17 Taylor, M. K. *et al.* Tuning the Adsorption-Induced Phase Change in the Flexible Metal–Organic Framework Co(bdp). *J. Am. Chem. Soc.* **138**, 15019-15026, doi:10.1021/jacs.6b09155 (2016).
- 18 Horcajada, P. *et al.* How Linker’s Modification Controls Swelling Properties of Highly Flexible Iron(III) Dicarboxylates MIL-88. *J. Am. Chem. Soc.* **133**, 17839-17847, doi:10.1021/ja206936e (2011).
- 19 Devic, T. *et al.* Functionalization in Flexible Porous Solids: Effects on the Pore Opening and the Host–Guest Interactions. *J. Am. Chem. Soc.* **132**, 1127-1136, doi:10.1021/ja9092715 (2010).
- 20 Ramsahye, N. A. *et al.* Influence of the Organic Ligand Functionalization on the Breathing of the Porous Iron Terephthalate Metal Organic Framework Type Material upon Hydrocarbon Adsorption. *J. Phys. Chem. C* **115**, 18683-18695, doi:10.1021/jp205369t (2011).
- 21 Kundu, T., Shah, B. B., Bolinois, L. & Zhao, D. Functionalization-Induced Breathing Control in Metal–Organic Frameworks for Methane Storage with High Deliverable Capacity. *Chem. Mater.* **31**, 2842-2847, doi:10.1021/acs.chemmater.8b05332 (2019).
- 22 Mason, J. A. *et al.* Methane storage in flexible metal–organic frameworks with intrinsic thermal management. *Nature* **527**, 357-361, doi:10.1038/nature15732 (2015).
- 23 Zhu, A.-X. *et al.* Tuning the Gate-Opening Pressure in a Switching pcu Coordination Network, X-pcu-5-Zn, by Pillar-Ligand Substitution. *Angew. Chem. Int. Ed.* **58**, 18212-18217, doi:10.1002/anie.201909977 (2019).

- 24 Horike, S., Inubushi, Y., Hori, T., Fukushima, T. & Kitagawa, S. A solid solution approach to 2D coordination polymers for CH₄/CO₂ and CH₄/C₂H₆ gas separation: equilibrium and kinetic studies. *Chem. Sci.* **3**, 116-120, doi:10.1039/C1SC00591J (2012).
- 25 Fukushima, T. *et al.* Solid Solutions of Soft Porous Coordination Polymers: Fine-Tuning of Gas Adsorption Properties. *Angew. Chem. Int. Ed.* **49**, 4820-4824, doi:10.1002/anie.201000989 (2010).
- 26 Zhang, J.-P., Zhu, A.-X., Lin, R.-B., Qi, X.-L. & Chen, X.-M. Pore Surface Tailored SOD-Type Metal-Organic Zeolites. *Adv. Mater.* **23**, 1268-1271, doi:10.1002/adma.201004028 (2011).
- 27 Henke, S., Schmid, R., Grunwaldt, J.-D. & Fischer, R. A. Flexibility and Sorption Selectivity in Rigid Metal–Organic Frameworks: The Impact of Ether-Functionalised Linkers. *Chem. Eur. J.* **16**, 14296-14306, doi:10.1002/chem.201002341 (2010).
- 28 He, Y., Krishna, R. & Chen, B. Metal–organic frameworks with potential for energy-efficient adsorptive separation of light hydrocarbons. *Energy Environ. Sci.* **5**, 9107-9120, doi:10.1039/C2EE22858K (2012).
- 29 Duan, X., Cui, Y., Yang, Y. & Qian, G. A novel methoxy-decorated metal–organic framework exhibiting high acetylene and carbon dioxide storage capacities. *CrystEngComm* **19**, 1464-1469, doi:10.1039/C6CE02291J (2017).
- 30 Pang, J. *et al.* A porous metal-organic framework with ultrahigh acetylene uptake capacity under ambient conditions. *Nat. Commun.* **6**, 7575, doi:10.1038/ncomms8575 (2015).
- 31 Cai, J. *et al.* An amino-decorated NbO-type metal–organic framework for high C₂H₂ storage and selective CO₂ capture. *RSC Adv.* **5**, 77417-77422, doi:10.1039/C5RA12700A (2015).
- 32 Wang, S.-Q. *et al.* High Working Capacity Acetylene Storage at Ambient Temperature Enabled by a Switching Adsorbent Layered Material. *ACS Applied Materials & Interfaces*, doi:10.1021/acsami.1c06241 (2021).
- 33 Sun, X. *et al.* Tuning the gate opening pressure of a flexible doubly interpenetrated metal–organic framework through ligand functionalization. *Dalt. Trans*, **47**, 13158-13163, doi:10.1039/C8DT02544D (2018).

- 34 Schwedler, I. *et al.* Mixed-linker solid solutions of functionalized pillared-layer MOFs – adjusting structural flexibility, gas sorption, and thermal responsiveness. *Dalt. Trans*, **45**, 4230-4241, doi:10.1039/C5DT03825A (2016).
- 35 Foo, M. L., Matsuda, R. & Kitagawa, S. Functional Hybrid Porous Coordination Polymers. *Chem. Mater.* **26**, 310-322, doi:10.1021/cm402136z (2014).
- 36 Lescouet, T., Kockrick, E., Bergeret, G., Pera-Titus, M. & Farrusseng, D. Engineering MIL-53(Al) flexibility by controlling amino tags. *Dalt. Trans*, **40**, 11359-11361, doi:10.1039/C1DT11700A (2011).
- 37 Chen, B. *et al.* A Microporous Metal–Organic Framework for Gas-Chromatographic Separation of Alkanes. *Angew. Chem. Int. Ed.* **45**, 1390-1393, doi:10.1002/anie.200502844 (2006).
- 38 Gu, Y. *et al.* Structural-Deformation-Energy-Modulation Strategy in a Soft Porous Coordination Polymer with an Interpenetrated Framework. *Angew. Chem. Int. Ed.* **59**, 15517-15521, doi:10.1002/anie.202003186 (2020).
- 39 Xiang, S., Zhou, W., Gallegos, J. M., Liu, Y. & Chen, B. Exceptionally High Acetylene Uptake in a Microporous Metal–Organic Framework with Open Metal Sites. *J. Am. Chem. Soc.* **131**, 12415-12419, doi:10.1021/ja904782h (2009).
- 40 Fukushima, T. *et al.* Modular Design of Domain Assembly in Porous Coordination Polymer Crystals via Reactivity-Directed Crystallization Process. *J. Am. Chem. Soc.* **134**, 13341-13347, doi:10.1021/ja303588m (2012).
- 41 Lescouet, T. *et al.* Homogeneity of flexible metal–organic frameworks containing mixed linkers. *J. Mater. Chem.* **22**, 10287-10293, doi:10.1039/C2JM15966J (2012).
- 42 Ghoufi, A., Maurin, G. & Férey, G. Physics Behind the Guest-Assisted Structural Transitions of a Porous Metal–Organic Framework Material. *J. Phys. Chem. Lett.* **1**, 2810-2815, doi:10.1021/jz1011274 (2010).
- 43 Coudert, F.-X., Jeffroy, M., Fuchs, A. H., Boutin, A. & Mellot-Draznieks, C. Thermodynamics of Guest-Induced Structural Transitions in Hybrid Organic–Inorganic Frameworks. *J. Am. Chem. Soc.* **130**, 14294-14302, doi:10.1021/ja805129c (2008).
- 44 Bousquet, D., Coudert, F. X. & Boutin, A. Free energy landscapes for the thermodynamic understanding of adsorption-induced deformations and structural transitions in porous materials. *J. Chem. Phys.* **137**, 044118, doi:10.1063/1.4738776 (2012).

- 45 Kitaura, R., Fujimoto, K., Noro, S.-i., Kondo, M. & Kitagawa, S. A Pillared-Layer Coordination Polymer Network Displaying Hysteretic Sorption: $[\text{Cu}_2(\text{pzdc})_2(\text{dpyg})]_n$ (pzdc= Pyrazine-2,3-dicarboxylate; dpyg=1,2-Di(4-pyridyl)glycol). *Angew. Chem. Int. Ed.* **41**, 133-135, doi:10.1002/1521-3773(20020104)41:1<133::aid-anie133>3.0.co;2-r (2002).

Methods

Materials. All chemicals were used as received without any further purification., 1,4-benzenedicarboxylic acid, 2-amino-1,4-benzenedicarboxylic acid, 2-nitro-1,4-benzenedicarboxylic acid, 4,4'-bipyridine were purchased from TCI. Zinc nitrate hexahydrate, Ethanol (EtOH), dimethylformamide (DMF) and other materials were purchased from Nacalai Tesque.

Synthesis of Zn-CAT and Zn-CAT-(X)_n MOF series. The syntheses of **Zn-CAT** and **Zn-CAT-(X)_n** series ($n = 0$ to 100% and $X = -NH_2, -NO_2$) were conducted following a method previously published and can be produced in 100 g scale.³⁷ Specifically, 1,4-benzenedicarboxylic acid is dissolved with the functionalized 1,4-benzenedicarboxylic acid (total 2 eq, 20 mmol) in DMF (concentration [**bdc linker**] = 0.15 M) at 373.15 K for 15 min. An ambient solution of Zn(NO₃).6H₂O (2 eq, 5.94 g, 20 mmol) in DMF (concentration [**metal**] = 0.4 M) was added to the stirring mixture at 373.15 K for 10 min. 4,4'-bipyridine (1 eq, 1.56 g, 10 mmol) is dissolved at room temperature in EtOH (concentration [**pillar**] = 0.1 M) and added to the reaction mixture. The mixture was kept at 373.15 K for 24 h. After cooling down to room temperature, the resulting precipitated is collected *via* centrifugation and washed three time with DMF (3 x 40 mL) and three times with EtOH (3 x 40 mL). The material is dried under vacuum at 323.15 K for 12 h to give a white/yellow powder in ~ 90 to 98 % yields (6 to 6.9 g).

¹H Nuclear Magnetic Resonance (NMR) spectra. Each MOFs were dissolved in 0.75 mL of DMSO-d⁶ and 10 μL of deuterated TFA. ¹H NMR spectra were recorded at 298.15 K at 400 MHz, where chemical shifts (δ in ppm) were determined with respect to tetramethylsilane (TMS) as an internal reference.

Thermogravimetric Analysis (TGA). Thermal stability of all MOFs were measured under nitrogen flux with a heating rate of $5 \text{ K}\cdot\text{min}^{-1}$ from 303.15 K to 773.15 K on a Perkin Elmer STA 6000 Thermo Gravimetric Analyzer.

Powder X-ray diffraction (PXRD). PXRD measurements were performed on a Rigaku SmartLab X-ray diffractometer using Cu-K α radiation ($\lambda = 1.54178 \text{ \AA}$) in the 2θ range of $3\text{--}40^\circ$ with a scanning rate of $5^\circ\cdot\text{min}^{-1}$.

Ultraviolet-visible Absorption (UV) spectroscopy. UV spectra of all materials were measured on a JASCO V670 spectrophotometer from 700 to 200 nm. Samples were previously heated at 423 K under vacuum for 12 h before measurements.

Scanning Electron Microscopy (SEM) analyses. SEM images were collected with HITACHI SU5000 microscope using 3.0 kV acceleration voltage and 5 mm working distance. Samples were directly deposited on a carbon conductive carbon tape.

Single crystal X-ray diffraction. Measurements of single crystal X-ray diffraction data for as-synthesised and activated **Zn-CAT-(NO₂)₁₀₀** were collected on the beamline BL02B1 at the Japan Synchrotron Radiation Research Institute with 0.41270 \AA radiation at 100 K and 195 K respectively. Crystals were extracted from a mixture DMF/EtOH into oil and mounted onto the goniometer for data collection. The structures were solved using *SHELXT*. Structure solution and refinement was performed within *SHELXL* on *Olex2*. Crystal information and details relating to the structural refinements are presented in Supplementary **Table 1 & 2**. Crystallographic data for as-synthesized and activated **Zn-CAT-(NO₂)₁₀₀** structures have been deposited in the Cambridge Structural Database with CCDC numbers 2036574 -2036575.respectively.

Single gas adsorption isotherms. MOF samples were prior activated through thermal activation at 423 K for 12 h before measurement. The adsorption isotherms were measured with BELSORP-CRYO (C₂H₂ and CO₂) and BELSORP-MAX (C₂H₂, CO₂, CH₄ and O₂) volumetric adsorption equipment from Bel Japan. Targeted relative pressures in the range of 0.01-100 kPa were defined and limits of excess and allowance amount were set to 5 and 10 cm³.g⁻¹, respectively. Equilibrium conditions for each point were: 0.03 % pressure change within 300 s. The dead volume was determined using helium gas.

Gate opening and closing pressure and total capacity determination The gate pressure points were determined at the inflection point of the adsorption and desorption isotherms. The total capacity reported are the maximum amount of gas adsorbed by the material.

In-situ PXRD coupled with gas sorption measurements. The measurements were performed on BELSORP-18PLUS (MicrotracBEL, Japan, Corp.) automated volumetric sorption analyzers, equipped with cryostat temperature controllers. The in-situ PXRD/adsorption measurements were carried out using a Rigaku SmartLab with Cu-K α radiation connected to BELSORP-18PLUS volumetric adsorption equipment. Those apparatuses were synchronized with each other and each PXRD pattern was obtained at each point of the sorption isotherms. The samples were prior activated through external thermal activation at 423 K for 12 h and further 2 h internal activation at 423 K before measurement.

Acetylene high pressure storage test set-up measurements. The experimental set-up used for acetylene storage measurements is shown in Supplementary **Fig. 37**. The gas manifold consisted of two lines fitted with mass flow controller. One line is used to feed an inert gas, in our case, helium gas is used as reference gas before each experiment and as gas purge after each acetylene measurement. The other line, contains pure acetylene gas. In a typical experiment, 10 g of

adsorbent powder was activated under vacuum at 423 K in a separate oven for 12 h. The vessel is filled with helium and plugged in the set-up. Before starting each experiment, the column is evacuated and heated at 423 K for 2 h before the acetylene filling at a flow rate of $50 \text{ cm}^3 \cdot \text{min}^{-1}$. The acetylene filling process was performed at low temperature (273 K or 243 K). After reaching the maximum loading, the vessel was slowly warmed to 290 K, 298 K or 310 K. The acetylene excess amount was released during the heating process. After filling, the desorption is made by vacuum pump until complete release of the gas.

Additional Information

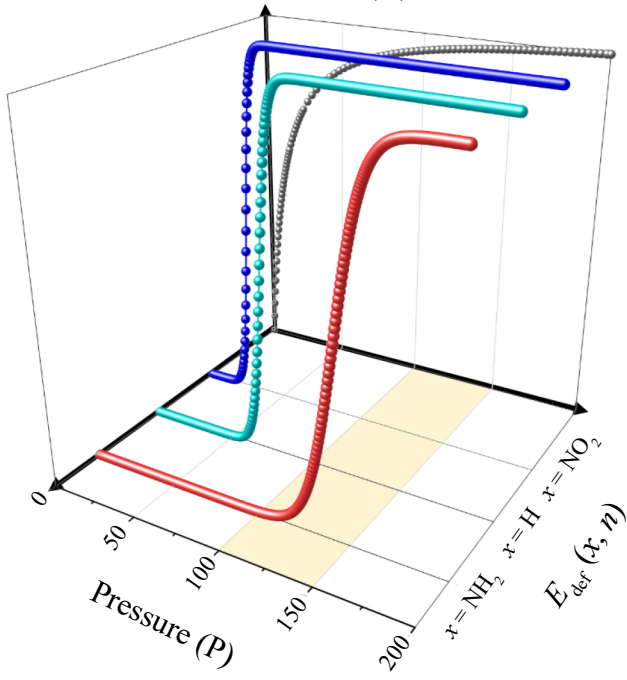
Data availability X-ray crystallographic data have been deposited at the Cambridge Crystallographic Data Centre (<http://www.ccdc.cam.ac.uk/>) with reference numbers CCDC 2036574-2036575. A copy of the data can be obtained free of charge via <https://www.ccdc.cam.ac.uk/structures/>. All other data supporting the findings of this study are available within the article and its Supplementary Information. Data are also available from the corresponding author upon reasonable request.

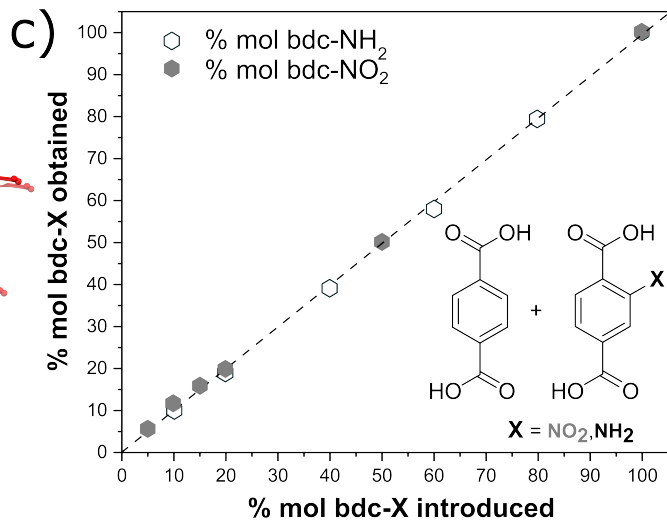
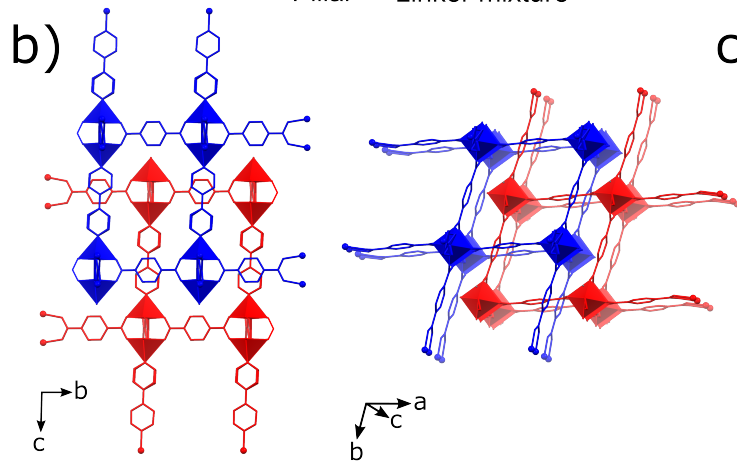
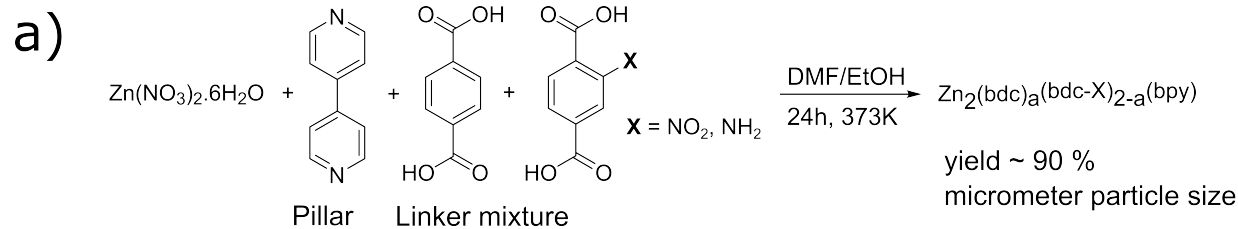
Supplementary Information The online version contains supplementary material available at <http://doi.org/xxxxxxx>

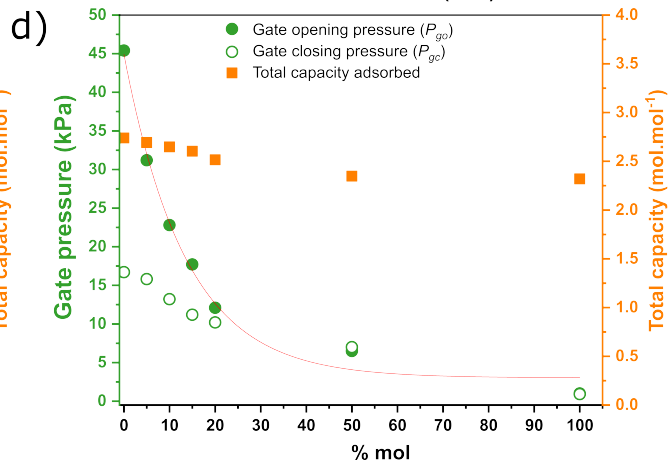
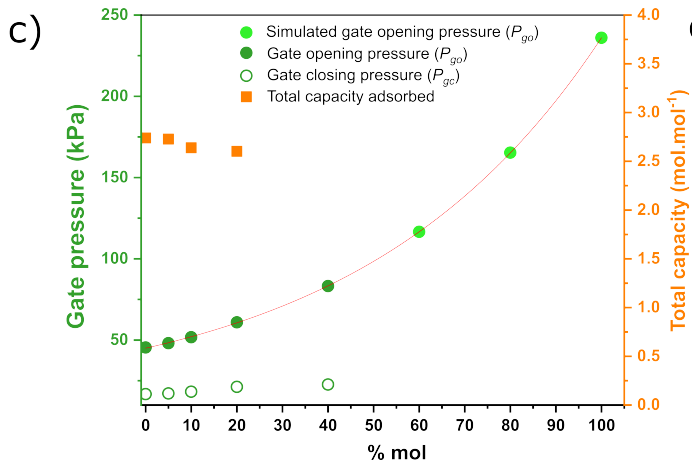
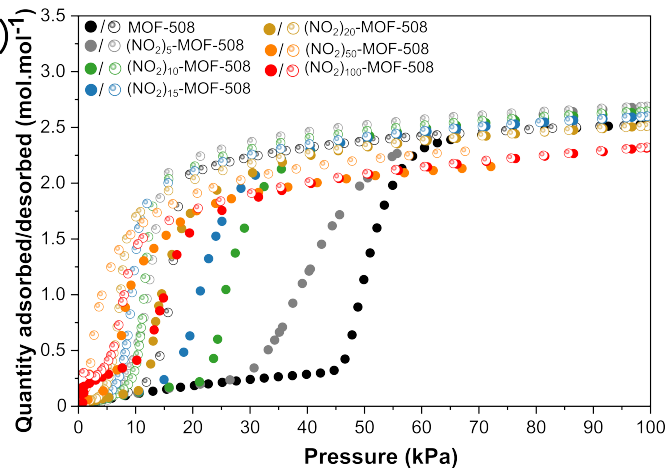
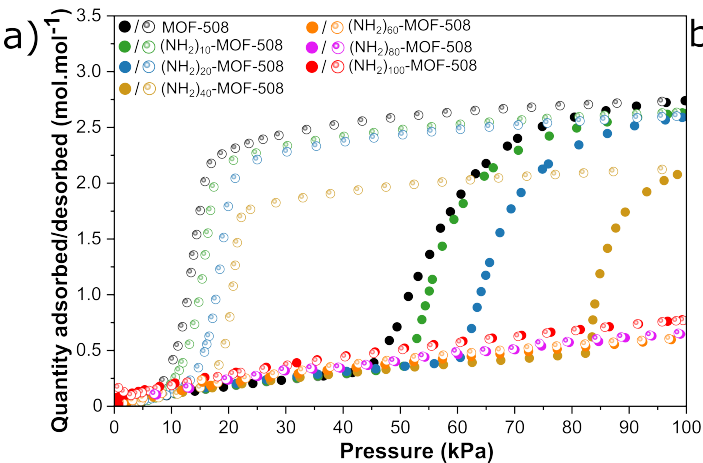
Correspondance and requests for materials should be addressed to S.K.
(kitagawa@icems.kyoto-u.ac.jp)

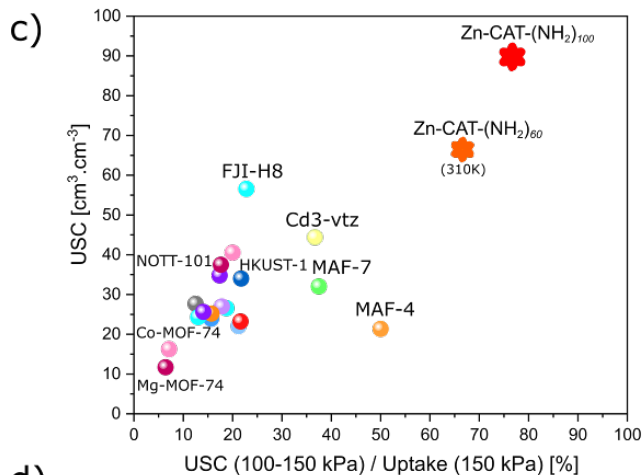
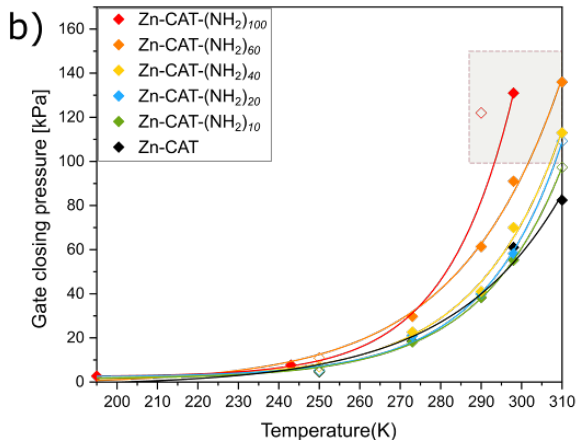
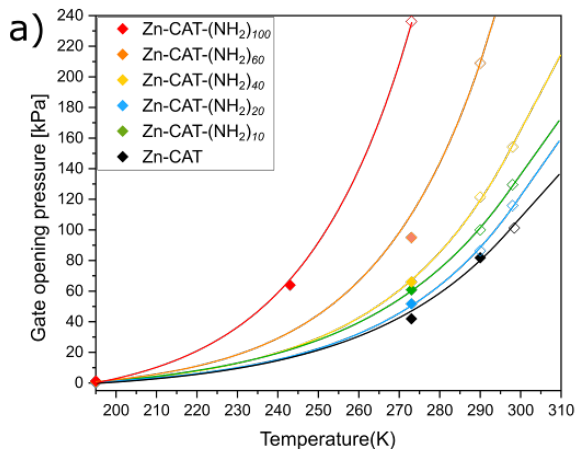
Reprint and permission information is available at www.nature.com/reprints. and the details are available in the online version of the paper. Readers are welcome to comment on the online version of this paper.

Adsorbed amount (A)









d)

Standard S11/B11 cylinder	9.6L	New system MOF filler	Free-solvent acetylene cylinder	Solvent acetylene cylinder
Filling method		Adsorption		Dissolution
Weight (kg)		7.4	~ 9.5	14
Acetylene volume (L)		~ 700	19	1400
Solvent concentration (wt%) ^a		None	None	3.3
Storage pressure (kPa)		150	147	1900

^(a) Solvent used: acetone at 25 °C